Study of MgB_2 ultra-thin films in submicron size bridges

Evgenii Novoselov, Naichuan Zhang and Sergey Cherednichenko

***Abstract*— We discuss a custom built hybrid physical chemical vapour deposition (HPCVD) system for MgB_2 ultra-thin film deposition: construction, deposition process development, and optimization. Achieved films on SiC substrates have a critical temperature (T_c) ranging from 35K (10nm thick films) to 41K (40nm thick films). The 20nm thick unpatterned film had a room temperature resistivity of 13μΩ·cm, whereas it becomes 50μΩ·cm in sub-micrometer size bridges with a critical current density J_c (4.2K) up to 1.2×10^8A/cm^2. The lower value of resistivity corresponds to the higher of both T_c and J_c. The surface roughness, measured with an atomic force microscope (AFM), is approximately 1.5nm.**

***Index Terms*—hot-electron bolometer, HPCVD, magnesium diboride, superconductivity, thin film.**

I. Introduction

Heterodyne receivers are required in order to achieve a high spectral resolution in sub-mm astronomy observations [1]. The most sensitive mixers used in heterodyne instruments for the frequency range above 1THz are superconducting hot-electron bolometer (HEB) mixers [2]–[4]. Widely used NbN HEB mixers provide a noise temperature close to ten times the quantum limit and a gain bandwidth (GBW) of 2-3GHz. However, for many astronomical tasks a larger GBW is required [5].

In order to improve the IF bandwidth of HEB mixers, materials with a higher critical temperature (T_c) that provide a shorter electron-phonon interaction time, would be of advantage. MgB_2 is an example of such a material [6]. HEB mixers made from molecular beam epitaxy (MBE) grown MgB_2 films on sapphire have been successfully realized and tested [7]–[10]. Unfortunately, with the MBE process a great reduction of T_c occurs for films thinner than 20nm, whereas for HEB mixers both a high T_c and a small thickness are desirable. A hybrid physical chemical vapour deposition (HPCVD) method developed for MgB_2 thin films can provide ultra-thin superconducting films of high quality [11], [12]. With such films a gain bandwidth of up to 10GHz and HEB operation up to 20K [13] (where compact cryocoolers could be used) can be achieved. This study addresses optimization of the HPCVD method for HEB mixer fabrication.

II. MgB_2 Thin Films

Superconductivity in MgB_2 was reported in 2001 [14]. It immediately triggered a great interest to MgB_2 film deposition. Several methods for deposition of thin MgB_2 films have been demonstrated, including pulsed laser deposition (PLD), MBE, and HPCVD.

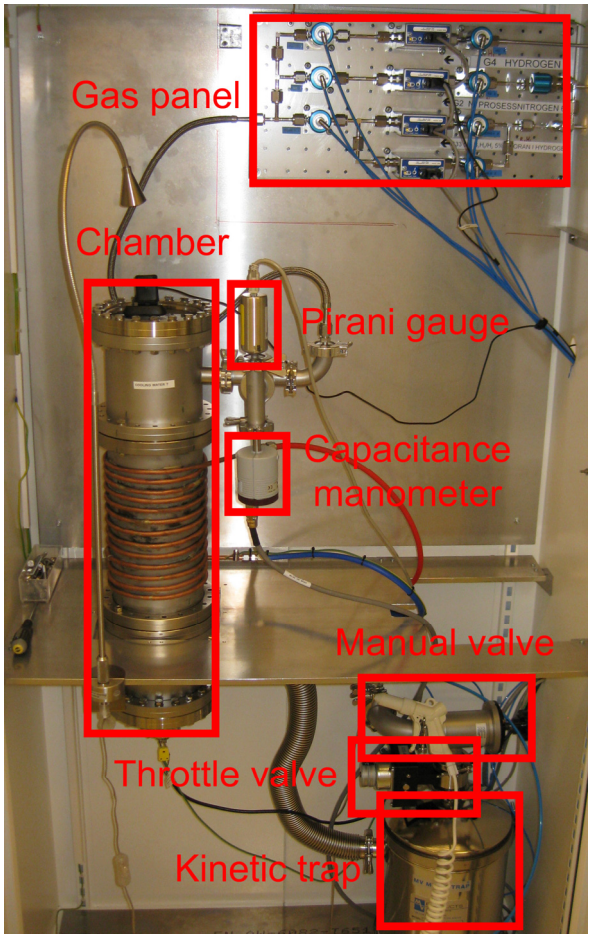

Fig. 1. Chalmers in-house built MgB_2 HPCVD system.

MgB_2 is a conventional intermetallic compound superconductor with the highest T_c of 39K reported so far. An electron-phonon interaction time of 3ps (much shorter, in comparison to the one in NbN (12ps)) was measured in thin MgB_2 films [15]. MgB_2 consists of hexagonal magnesium (Mg) layers with honeycomb boron (B) layers in between. The hexagonal unit cell has the following lattice constants a=3.086Å, c=3.524Å. Therefore, the most suitable substrates

This work was supported by the European Research Council (ERC).

E. Novoselov, N. Zhang and S. Cherednichenko are with the Department of Microtechnology and Nanoscience (MC2), Chalmers University of Technology, SE-41296 Göteborg, Sweden (e-mail: evgenii@chalmers.se).

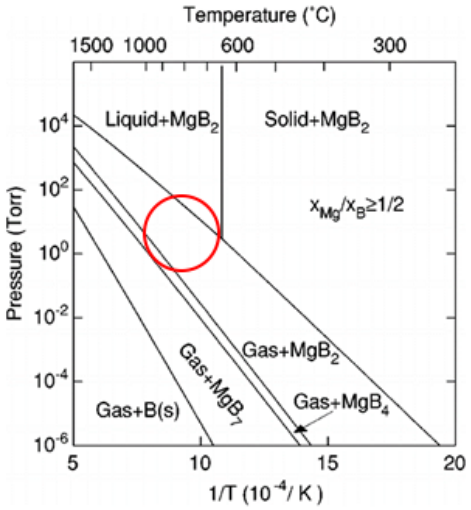

Fig. 2. Pressure–temperature phase diagram for the Mg-B [18].

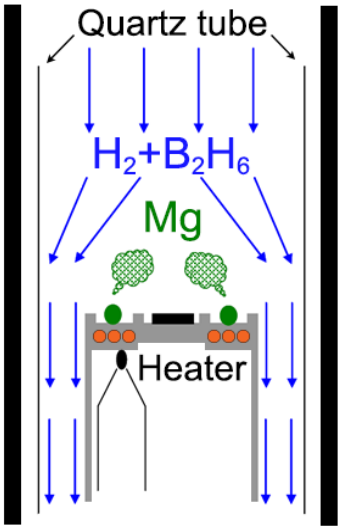

Fig. 3. Schematic drawing of the HPCVD system's deposition chamber.

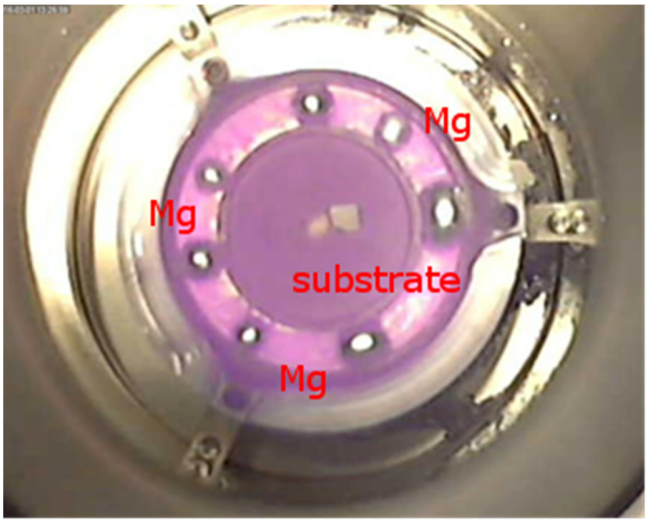

Fig. 4. Chamber view during the deposition process.

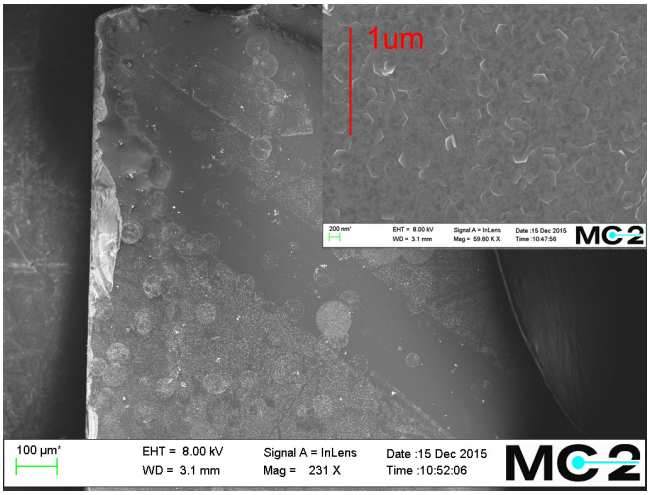

Fig. 5. SEM image of Film 2 (20sccm 120s 40Torr) deposited on the sapphire substrate.

for MgB_2 thin film deposition are sapphire (Al_2O_3) and silicon carbide (SiC). For Al_2O_3 with the lattice constant of a=4.758Å Al_2O_3/ MgB_2 lattice mismatch is ~11% (30° in-plane rotation). For SiC (a=3.070Å) the lattice mismatch is even smaller (~0.42%). A better film/substrate lattice match reduces the number of defects in a bottom layer of the film. This leads to a better phonon transparence of the film-substrate interface. Thinner films provide a shorter phonon escape time from the film into the substrate, which is another important limiting factor for the HEB mixers gain bandwidth. Films as thin as 10nm were reported in [16] with a T_c of 36K (almost the same as for the bulk). No devices made using such films have been reported to date.

Local Oscillator power is known to increase with the HEB in-plane dimensions. Therefore, a micrometer and sub-micrometer size HEBs are usually fabricated in order to match the reduced output power of THz LO sources. This maximum size restriction imposes a strong limitation on the superconducting film morphology. Uniform films with a smooth surface are of advantage for reproducible HEB mixer fabrication. As-deposited thin MgB_2 films have previously been characterized with a high concentration of defects leading to a high resistivity and a low critical current density (J_c). This is particularly seen in microstructured (patterned) films. Recently, a method for obtaining thin films from thinning down thick films was reported [17]. In that work films as thin as 2.9nm with a T_c of 36K were made. However, it is still a question how this films will behave when patterned in submicron structures.

Our goal was to investigate degradation of superconducting properties (T_c and J_c) as well as normal state resistance for ultra-thin MgB_2 films in sub-micrometer size bridges, similar to those used in HEB mixers.

III. Chalmers HPCVD System

A custom made HPCVD system was built at Chalmers University of Technology for deposition of MgB_2 thin films. The system photo is shown in Fig. 1. Gases (hydrogen (H_2), diborane (B_2H_6) (5% in H_2), and purging nitrogen (N_2)) are supplied to the deposition chamber using a computer controlled gas panel consisting of pneumatic valves and mass-flow

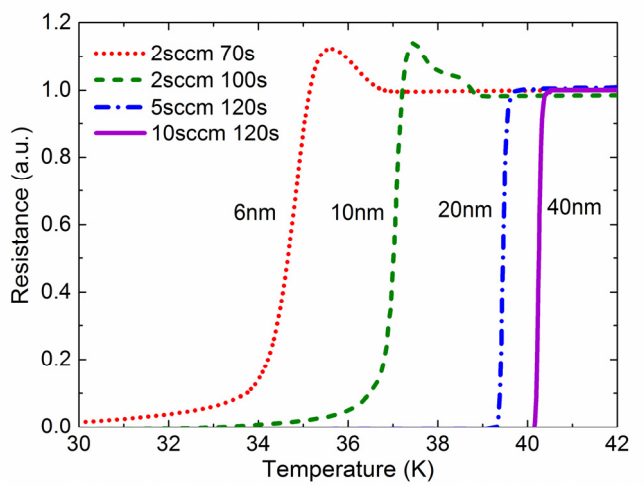

Fig. 6. Normalized R-T curves for MgB_2 films deposited at various B_2H_6 gas flows with different deposition times. Deposition pressure is 20mTorr.

TABLE I
MgB_2 HEB SIZE (WxL), THICKNESS (D), CRITICAL TEMPERATURE (T_c), RESISTIVITY IN MICROSTRUCTURE (ρ_{300K}), RESISTIVITY IN FILM (ρ_{FILM}) AND CRITICAL CURRENT DENSITY AT 4.2K (J_c).

#	WxL (μm^2)	D (nm)	ρ_{300K} (ρ_{film}) ($\mu\Omega$·cm)	T_c(K)	J_c (10^7A/cm^2)
E2	1×1	30 [1)]	117-131 [3)] (12)	39.4-39.6	8.8-11.9
E3	0.8×0.8 or 0.5×0.5	20 [2)]	40-47 (13)	38.6-39.2	11.6-12.0
E8	0.5×0.5 or 0.3×0.3	10 [2)]	46-87 (35)	32.5-34.2	1.2-3.2

1) Determined by deposition rate
2) Measured by transmission electron microscope (TEM)
3) Rougher film deposited at 40Torr

controllers (MFCs). The MgB_2 deposition occurs only when B_2H_6 flows through the chamber. At 650°C solid Mg pellets melt providing the required high Mg gas pressure. Above the hot substrate B_2H_6 decomposes and reacts with Mg. As a result, MgB_2 is deposited on the substrate, whereas excess Mg remains in the gas phase. The region where this process occurs is shown with a circle on the phase diagram (see Fig. 2). As one can see, in order to form MgB_2 both the Mg partial pressure and the temperature should fall in a quite tight area in the phase diagram.

A pirani gauge is mounted on the deposition chamber to monitor the pressure during pumping to the base pressure. A capacitance manometer and a throttle valve are connected to a pressure controller to set the desired process pressure. A kinetic trap follows the deposition chamber in order to protect both the throttle valve and the fore-vacuum pump from residuals of the deposited material carried by the gas flow. The fore vacuum pump and the scrubber used for B_2H_6 disposal are placed outside the main cabinet in the utility room. For safety reasons H_2 gas is cleaned from B_2H_6 is mixed with N_2 to prevent formation of dangerously explosive concentrations of the oxyhydrogen.

A schematic of the MgB_2 HPCVD system chamber is presented in Fig. 3. A quartz tube prevents material deposition

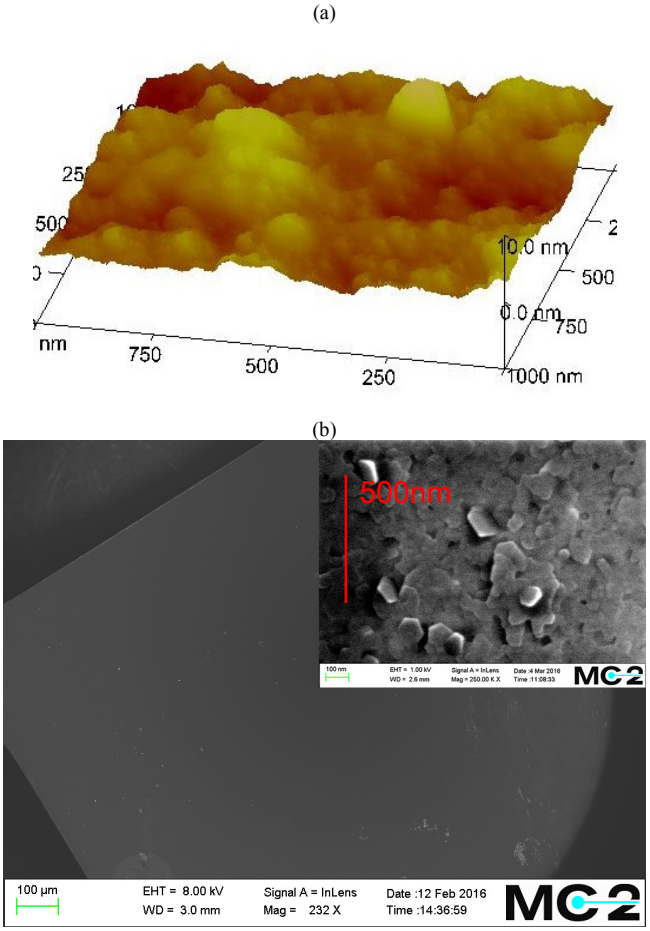

Fig. 7. (a) AFM and (b) SEM images of Film 37 (10sccm 120s 40Torr) deposited on SiC substrate.

on water cooled chamber metal walls. Both the substrate and the pieces of solid Mg are placed on the heater. A coaxial heating wire is clamped between the upper and the bottom parts of the heater such that it occurs just under the area where magnesium is placed. In contrast to the previously presented resistive heater designs the coaxial wire itself is hidden inside the heater, which reduces contamination of working parts during the deposition and increases the heater life time. Due to a finite temperature gradient the temperature of the central part where the substrate is placed is 50K lower than under Mg pellets. A thermocouple is attached to the bottom part of the holder to monitor the temperature during the deposition process.

The sequence for MgB_2 thin film deposition is as following. First, the chamber is pumped till the base pressure is reached (~10^{-3}Torr). Then, it is flushed with H_2 and pumped again to the base pressure. The chamber is filled with H_2 (400sccm) to a pressure of 20-40Torr set by the throttle valve. Mg and the substrate are heated to about 690-720°C, which is above the melting point of Mg (650K). After this, the B_2H_6 mixture is turned on. The chamber view during the deposition process is presented in Fig. 4. After the deposition the heater is turned off and the substrate is cooled down. Before the chamber is opened, it is flushed several times with N_2 in order to clean the chamber from remaining B_2H_6.

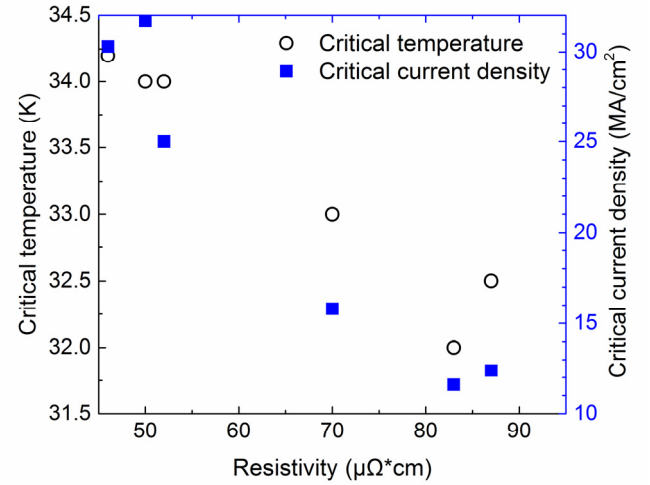

Fig. 8. Critical temperature and critical current density versus resistivity of the film measured for the devices from batch E8.

IV. Thin Films Characterization

First MgB_2 thin films were deposited on sapphire substrates. The films thickness is defined by the B_2H_6 flow rate and the flow time. The film thickness was measured both with a contact profilometer and an atomic force microscope (AFM). For this purpose, MgB_2 is etched away on a fraction of the substrate using HCl acid (15-40s etching time, depending on the thickness). The T_c of deposited films ranged from 33K (15nm) to 37K (40nm) and showed a distinct double transition. Films were very inhomogeneous with lots of spots and particles (see Fig. 5). HPCVD films grow in Volmer-Weber mode and distinct crystallites are seen on the SEM image in the inset in Fig. 5. Another important parameter is the residual resistance ratio ($RRR=R_{300K}/R_{50K}$). For MgB_2 films on sapphire substrates RRR was 1.5-2.5 indicating a high concentration of defects (RRR is about 10 for clean MgB_2 films [12]).

MgB_2 films deposited on SiC substrates had a T_c ranging from of 35K (10nm thick) to 41K (40nm thick) (see Fig. 6). However, some problem with the film surface cleanness and homogeneity remained. Crystals with different crystal structure were observed on the film surface with the SEM. Formation of such crystallites could be due to insufficient Mg pressure (Fig. 2). After an increase of the Mg amount the problem with the film inhomogeneity was solved. RRR of the films deposited on SiC substrates was ranging from 2 to 6 indicated improvement of film quality. Optimized films were also studied with atomic force microscope (AFM). A 3D plot recorded with the AFM is shown in Fig. 7, together with a SEM image. The measured roughness was about 1.5nm, which is lower than for previously reported ultra-thin HPCVD MgB_2 films [16]. The low roughness is one of the most important characteristics affecting fabrication of micro- and nanostructures on thin films. We observed that reduction of the deposition pressure from 80Torr to 20Torr continuesly leads to smoother film surfaces. For deposition pressures above 30Torr a droplet formation is observed in the deposition chamber, which probably leads to a rougher film. Therefore, all our latest films were made with a pressure of 20Torr.

Film parameters in microstructure were studied in several batches of HEBs fabricated using either photo- or e-beam lithography, metal evaporation and ion-beam milling techniques. MgB_2 films were covered with a 20nm Au layer in another machine directly after the deposition. This Au layer was used both to protect the deposited film from degradation in the atmosphere as well as to be able to use the same fabrication process previously developed for HEBs made from MBE films [9], [10]. Measured HEB parameters for three batches made with e-beam lithography are summarised in Table I.

One of the critical film characteristics is the thickness. There are several techniques to measure the conductive film thickness: mechanical and optical surface profilers, AFM, TEM, ellipsometry, etc. Ellipsometry is a non-invasive method (the film is presenrved for further studies). However, it requires preliminary knowledge of the MgB_2 film optical properties. Most of our film thickness data originates from the mechanical profilometer and AFM, which both require a film/substrate step to be defined with an etching process. Two samples have also been studied with a Transmission Electron Microscope (TEM) (E3 and E8 in Table I), where the film thickness of 20nm and 10 nm were measured, respectively.

At room temperature the unpatterned film sheet resistance is measured with a four-point probe technique. With the film thickness knowledge (see above) the room temperature resistivity for unpatterned films of 20nm an 10nm thick was calculated to be 13μΩ·cm and 35μΩ·cm, respectively. These values correspond to the resistivity for the film of the same thicknesses obtained with "thinning-down" technique [17]. Resistivity obtained from resistance of sub-micrometer size bridges (see Table I) was approximately 40-50μΩ·cm (20nm thick film) and 46-87μΩ·cm (10nm thick film). It is a factor of 2 higher than in [17], hovewer we used much smaller bridge dimensions.

To better understand the reasons for an increased resistivity in thin films, the critical current density has to be discussed. As one can observe from Fig. 6 and Table I, the critical temperature for 10nm and 20nm thick films is 37K and 39K respectively. Whereas T_c for the 20nm film (E3) remains the same in microbidges, for the 10nm thick film T_c is reduced to 32-34K. Nevertherless, both films show excellent superconducting transition. The ciritical current density is obtained from IV characteristics of microbridges. For the 30nm and 20nm thick films J_c is at about $1\times10^8 A/cm^2$ (4.2K), hence is one of the highest critical current densities reported for MgB_2 (>10% of the de-pairing current). Even in the 10nm film the critical current density is $(1\text{-}3)\times10^7 A/cm^2$, which is the same as for thinned down films [17]. The fact that our as-deposited films have similar resistivity and the same (or higher) J_c can be possibly explained by the lower deposition rate in our HPCVD system as compared to [17]. Lower deposition rates facilitate more uniform MgB_2 film growth [20].

As mentioned above the critical current density in microbridges made from a 10nm thin film is lower than for thicker films. However, it is aproximatly a factor of 10 higher then for previosly reported microbidges made from MBE and HPCVD grown MgB_2 films [10], [13]. The high yield above 75% allowed for the study of correlation between the resistivity

and the critical density for the devices from the same batch (Fig. 8). The lower resistivity corresponds to the higher critical current density. The same behavior is obseerved also for the critical temperature of the devices (see Fig. 8). These results suggest that the 10nm film is quite inhomogenius over the substrate area.

In order to study how the thinning down by Ar^+ ion-beam milling affects our HPCVD MgB_2 films, three films of various thickness were fabricated. Films were deposited at 20Torr pressure with 120s deposition time, but under various B_2H_6 gas flow conditions: Film 61 (10sccm), Film 62 (20sccm), and Films 63 (5sccm). Ion etching was performed in 6 steps: 3 steps of 2min followed by 3 steps of 10min. The sheet resistance of each film was measured (at room temperature) with the 4-probe station just after the deposition and after each etching step (see Fig. 9). Based on the deposition parameters, Film 62 was expected to be twice thicker then Film 61, which is twice thicker than Film 63. As one can see Film 61 and Film 62 reach the same sheet resistance as Film 63 after 20min and 40min of etching, respectively. Film 63 was completely gone after about 20min of ion-beam milling. These etching times indicate the correctness of the film thickness relation assumption based on the gas flows.

Assuming that both the etching rate and the resistivity of the film were the same during the ion-beam milling process for all films the dependence of sheet resistance is calculated as $R_s=\rho/(d-r*t)$, where ρ is resistivity, d is film thickness, r is etching rate, and t is etching time. The fit to the experimental data gives the etching rate for selected parameters (2sccm Ar^+ flow, 13mA, 350V, 30º incidence) of about 1-1.2nm/min. The value corresponds to the etching rate observed during fabrication of HEBs. Film thicknesses for Film 61, Film 62, and Film 63 used for fitting are 40nm, 60nm, and 20nm, respectively. These values were predicted from relation between different gas flows used for film depositions based on previous film deposition results. For the future it is of great interest how HPCVD MgB_2 films would behave in submicron structure after the milling.

The film resistivity affects the design of HEB mixers. In order to provide the best performance, the resistance of HEB should be matched to the impedance of the integrated planar spiral antenna (100Ω). With a resistivity of about 50μΩ·cm (similar to the previously reported resistivity for the thin MgB_2 films [13]) an aspect ratio of HEB W/L should be less than 1. Together with a requirement from a limited available LO power (keeping a bolometer area small) it will lead to the reduction of bolometer width in the design (compared to HEB mixers made from MBE MgB_2 films [9], [10]). That will increase the contact resistance between the HEB and the metal antenna, which subsequently increases the receiver noise temperature.

V. Conclusion

The HPCVD system was successfully constructed and launched at Chalmers University of Technology. The low resistivity of ≈50μΩ·cm and the high critical current density of up to 1×10^8A/cm^2 indicates rather good quality of the achieved films. The micron and submicron size HEB mixers have already been already fabricated from these films and tested. The maximum IF frequency gain bandwidth of 6GHz was measured for $1\times1.5\mu m^2$ device made from 15nm thick MgB_2 film at 0.4THz [19]. However, further development of MgB_2 HPCVD process is required to improve stability and repeatability. Of the great interest is a study of a possibility to reduce the thickness of our films by ion-beam milling [17] and to pre-clean MgB_2 films prior the first protective Au layer deposition.

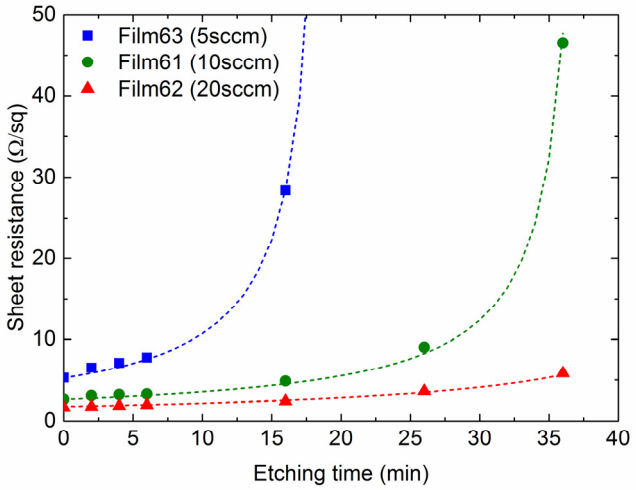

Fig. 9. Sheet resistance versus etching time. Deposition time and deposition pressure are 120s and 20Torr, respectively.

References

[1] H.-W. Hubers, "Terahertz Heterodyne Receivers," *IEEE J. Sel. Topics Quantum Electron.*, vol. 14, no. 2, pp. 378–391, Mar-Apr 2008.

[2] Th. de Graauw *et al.*, "The Herschel-Heterodyne Instrument for the Far-Infrared (HIFI)," *Astron. Astrophys.*, vol. 518, p. L6, Jul.-Aug. 2010.

[3] S. Heyminck *et al.*, "GREAT: The SOFIA high-frequency heterodyne instrument," *Astron. Astrophys.*, vol. 542, p. L1, Jun. 2012.

[4] D. Meledin *et al.*, "A 1.3 THz Balanced Waveguide HEB Mixer for the APEX Telescope," *IEEE Trans. Microwave Theory and Tech.*, vol. 57, pp. 89-98, Jan. 2009.

[5] A. F. Loenen et al., "Excitation of the molecular gas in the nuclear region of M82," *Astron. Astrophys.*, vol. 521, p. L2, Oct 2010.

[6] S. Cherednichenko *et al.*, "Terahertz mixing in MgB_2 microbolometers," *Appl. Phys. Lett.*, vol. 90, no. 2, pp. 023507-3, Jan. 2007.

[7] S. Bevilacqua *et al.*, "Low noise MgB_2 terahertz hot-electron bolometer mixers," *Appl. Phys. Lett.*, vol. 100, no. 3, p. 033504, Jan. 2012.

[8] S. Bevilacqua *et al.*, "Study of IF Bandwidth of MgB_2 Phonon-Cooled Hot-Electron Bolometer Mixers," *IEEE Trans. THz Sci. Technol.*, vol. 3, pp. 409-415, Jul. 2013

[9] S. Bevilacqua *et al.*, "MgB_2 Hot-Electron Bolometer Mixers at Terahertz Frequencies," *IEEE Trans. Appl. Supercond.*, vol. 25, p. 2301104, Jun. 2015.

[10] E. Novoselov et al., "Effect of the Critical and Operational Temperatures on the Sensitivity of MgB_2 HEB Mixers," *IEEE Trans. THz Sci. Technol.*, vol. 6, pp. 238-244, Mar. 2016.

[11] X. X. Xi et al., "Progress in the deposition of MgB_2 thin films," *Supercond. Sci. Technol.*, vol. 17, no. 5, pp. S196–S201, May 2004.

[12] X. X. Xi et al., "MgB_2 thin films by hybrid physical-chemical vapor deposition," *Phys. C, Supercond.*, vol. 456, no. 1/2, pp. 22–37, Jun. 2007.

[13] D. Cunnane *et al.*, "Characterization of MgB_2 Superconducting Hot Electron Bolometers," *IEEE Trans. Appl. Supercond.*, vol. 25, pp. 2300206, Jun. 2015.

[14] J. Nagamatsu *et al.*, "Superconductivity at 39K in magnesium diboride," *Nature*, vol. 410, no. 6824, pp. 63–64, Feb 2001.

[15] Y. Xu et al., "Time-Resolved Photoexcitation of the Superconducting Two-Gap State in MgB_2 Thin Films," *Phys. Rev. Lett.*, vol. 91, no. 19, p. 197004, Nov. 2003.

[16] M.A. Wolak et al., "Fabrication and characterization of ultrathin MgB_2 films for hot-electron bolometer applications," *IEEE Trans. Appl. Supercond.*, vol. 25, p. 7500905, Jun. 2015.
[17] N. Acharya et al., "MgB_2 ultrathin films fabricated by hybrid physical chemical vapor deposition and ion milling," *APL Mater.*, vol. 4, no. 8, p. 086114, Aug. 2016.
[18] Z.-K. Liu et al., "Thermodynamics of the Mg–B system: Implications for the deposition of MgB_2 thin films," *Appl. Phys. Lett.*, vol. 78, no. 23, pp. 3678-3680, Jun. 2001.
[19] E. Novoselov, N. Zhang and S. Cherednichenko, "MgB_2 hot electron bolometer mixers for THz heterodyne instruments," *Proc. SPIE*, vol. 9914, p. 99141N, Jul. 2016.
[20] C. Zhuang et al., "Surface morphology and thickness dependence of the properties of MgB_2 thin films by hybrid physical-chemical vapor deposition," *Supercond. Sci. Technol.*, vol. 23. no. 5, p. 055004, Apr. 2010.